Available online at www.sciencedirect.com
SCIENCE DIRECT
Polymer 47 (2006) 2460–2469
polymer
www.elsevier.com/locate/polymer

Ultrasonic oscillations induced morphology and property development of polypropylene/montmorillonite nanocomposites

Lijuan Zhao, Jiang Li, Shaoyun Guo *, Qin Du

The State Key Laboratory of Polymer Materials Engineering, Polymer Research Institute of Sichuan University, Chengdu 610065, China

Received 11 October 2005; received in revised form 9 January 2006; accepted 7 February 2006
Available online 28 February 2006

Abstract

Polypropylene/montmorillonite nanocomposites (PPCNs) with 3% organophilic montmorillonite (OMMT) content were prepared via ultrasonic extrusion. The objective of present study was to investigate the effects of ultrasonic oscillations in processing on the morphology and property development of PPCNs. XRD and TEM results confirmed the intercalated structure of OMMT in conventional nanocomposite (without ultrasonic treatment) and ultrasonicated nanocomposite, but ultrasonic oscillations could make silicate layers finely dispersed and a little exfoliated. According to SEM, the OMMT particles were evenly and finely dispersed in the ultrasonicated nanocomposite via ultrasonic oscillations, and the aggregation size of clay particles was about 100 nm, which is less than that in conventional nanocomposite. The crystalline dimension, crystalline morphology and the growth rate of crystallization in PPCNs were investigated by DSC and PLM, it was found that the OMMT particles and ultrasonic oscillations played an important role in the nucleation rate, crystallization temperature and spherulite size of PP matrix in nanocomposites. Compared with conventional nanocomposite, the mechanical properties of the ultrasonicated nanocomposite increased due to the improved dispersion of OMMT and diminished spherulite size. The thermal stability and the rheological behavior of PP and its nanocomposites were both studied by thermogravimetry and high pressure rheometer, respectively.

Keywords: Polypropylene; Montmorillonite; Nanocomposites

1. Introduction

In recent years, polymer/organic–inorganic nanocomposites have attracted great interests, due to their unique properties, typically exhibited by high modulus and increased strength [1–5], less thermal expansion coefficient and thermal stability [6–10] and enhanced ionic conductivity [11,12]. One of the most promising nanocomposite systems is the hybrid based on a polymer and a layered silicate such as montmorillonite (MMT). Layered silicates are dispersed in a polymer matrix in the form of reticular layers and with a lamellar aspect ratio between 100 and 1000. The properties of nanocomposites are strongly dependent on the final morphology of the material, especially the dispersion of the nanoparticles in the polymer matrix and levels of intercalation and exfoliation [10,13,14]. Therefore, how to disperse clay in polymer matrix finely and improve the degree of intercalation and exfoliation become an essential issue in order to obtain the expected properties of polymer/clay nanocomposites (PCNs), particularly for polymers without any polar groups in its backbone, such as polypropylene (PP), polyethylene (PE) etc. Since, pristine layered silicates contain hydrated Na^+ and K^+ ions, they are only compatible with hydrophilic polymers, such as PEO [15], PVA [16] and Nylon [17]. So it is difficult for the layered silicates to disperse in PP matrix. In general, two ways have been used to increase compatibility between polymers and layered silicates. One is to modify clay with alkylammonium, alkylphosphonium (C_{16}–C_{18}) or co-intercalated monomers [18–20] to make the clay surface organophilic and enlarge the space between the layers, which makes it possible for the clay to be intercalated and exfoliated. The other way is to blend PP with compatibilizer, such as maleic anhydride grafted PP (PP-*g*-MA) [21], PP-*g*-MA oligomer [22], PP–OH oligomer [23], antioxidant [24]. Usuki and Hasegawa [21–23] believed that the driving force of the intercalation originates from the interaction between maleic anhydride or hydroxy groups and the oxygen groups of the silicate through hydrogen bonding.

Nevertheless, much attention has been paid to clay modification or adding compatibilizers into blends. Recently some researchers have noted the role and importance of

* Corresponding author. Tel.: +86 28 857 69062; fax: +86 28 854 02465.
E-mail address: nic7702@scu.edu.cn (S. Guo).

0032-3861/$ - see front matter © 2006 Elsevier Ltd. All rights reserved.
doi:10.1016/j.polymer.2006.02.011

processing in preparing nanocomposites. Dennis [25] demonstrated the importance of the chemistry of the clay surface modification and melt intercalation. The degree of dispersion was interpreted in terms of the residence time distribution in the extruder and the intensity of shear. He also proposed a model for organoclay delamination about the role of both shear and time. Kim [26] studied the MMT crystal structure and lamellar orientation of PCNs using injection molding. He found that the crystal orientation of PP chains was different between polymer matrix and MMT layers.

Although melt intercalation has profound economic and environmental importance, comparatively, it is relatively tough over either in situ intercalative polymerization or polymer solution intercalation. Innovative assisted methods for melt intercalation are very necessary to be developed. In the preparation of nanocomposites, ultrasound has been widely applied to promote the dispersion of nanoparticles in polymer solution. However, a few reports have been observed for ultrasound assisted melt intercalation of clay in polymer matrix. Previous researches [27–29] found ultrasound could make nanoclays in low viscosity monomers in situ polymerization disperse uniformly, as well as for the direct dispersion of fillers prior in melt mixing [30–32]. Lee et al. [33] extended the application of ultrasound in the preparation of polymer-based nanocomposites. They directly introduced the power ultrasound into polymer melt, and found that in situ ultrasound of the polymer melt phase is an effective method to enhance the dispersion, intercalation, and exfoliation of nanoclays in thermoplastic-based nanocomposites. But their experiments were carried out in a Teflon cup. Through such a small-scale batch processing, it is not only incompatible with current industrial process, such as extrusion and injection molding, but also no enough samples was produced to measure the mechanical property of nanocomposites.

In this work, PP/montmorillonite nanocomposites (PPCNs) were prepared via ultrasonic extrusion technology. Ultrasonic oscillations produce local shear at melts so as to promote good dispersion of nanoparticles in polymer matrix or intercalation and exfoliation of clay. We have reported this preparative technology previously [34], in which three systems and some elementary results have been discussed in brief. In this paper, the microstructures of PPCNs were investigated by XRD, TEM and SEM. DSC and PLM were used to investigate the rate of crystallization and the crystalline morphology of PP, which greatly affected the final properties of composite. Viscosity values at low shear rate, thermal stability and mechanical properties of PP and PPCNs samples were also studied.

2. Experimental

2.1. Materials

The polypropylene (PP, EPS30R) was provided by Qilu Petroleum Chemical Company Ltd. Its melt flow index (MFI) is 1.0–2.5 g/10 min. Maleated polypropylene (PP-*g*-MA, GPM200) with 0.1 wt% MA content, prepared by reactive extrusion, was supplied by Ningbo Nengzhiguang New Materials Technology Co. Ltd. Organic montmorillonite (OMMT, DK1) modified with 16-C alkyl quaternary ammoniumwas supplied by Zhejiang Fenghong Clay Chemicals Co. All the materials were dried for 36 h at 80 °C before preparation of nanocomposites.

2.2. Preparation of PPCNs nanocomposites

The preparation of PPCNs was carried out in a special extrusion system with ultrasonic oscillations, which was designed by our lab. The schematic representation of this technology is shown in Fig. 1. The extrusion system consists of an extruder and a cylinder die where ultrasonic oscillations are generated. The maximum power output and frequency of the ultrasonic generator are 300 W and 20 kHz, respectively. The ultrasonic oscillations are in the direction parallel to the flow of the polymer melt. A pressure transducer and a thermocouple are installed at the die for continuous recording of the variation of pressure and temperature during extrusion. The resulting products were compression molded at 185–190 °C for 8 min into plate with a thickness of 1 or 4 mm. The pressure of compression molding was 15 MPa. The compositions and abbreviations of PPCNs are listed in Table 1.

2.3. Measurements and characterizations

X-ray diffraction analysis (XRD) was carried out in order to confirm whether the PPCNs were formed. Samples were scanned under 2θ ranging from 0.5 to 35° at a rate of 1 °/min using a Philip X Pert Pro MPD Diffractometer (Cu kα radiation, generator voltage = 40 kV, current = 40 mA).

To clarify the nanoscale structure of the intercalated PPCNs, a transmission electron microscope (TEM) (FEI PECNAI) was used, and it was operated at an accelerating voltage of 200 kV. The ultrathin sections with a thickness of 100 nm were cryogenically microtomed.

The morphology of PPCNs was also investigated by a Hitachi X-650 scanning electron micrograph (SEM, made in Japan). The tensile fractured samples were quenched in liquid nitrogen and cryogenically ruptured to obtain sections along the tensile direction, which were sputter coated with Au before SEM observation. In order to observe the dispersion of OMMT

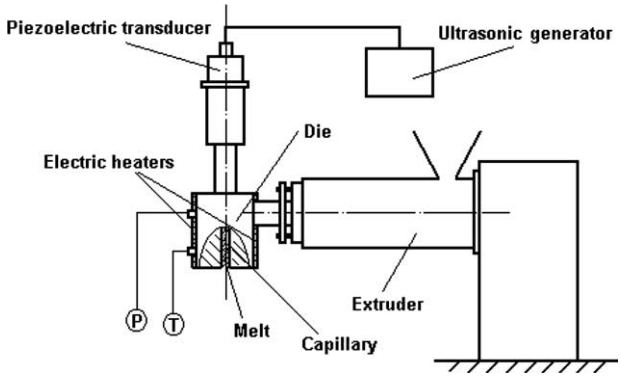

Fig. 1. Schematic diagram of ultrasonic oscillations extrusion system.

Table 1
Compositions and abbreviations of nanocomposites

Abbreviations	Contents in nanocomposites (wt%)			Processing conditions, ultrasonic power (W)
	Organophilic montmorillonite	Polypropylene	Maleated polypropylene	
PP	–	100	–	–
PPCN-0	3	88	9	–
PPCN-100	3	88	9	100

particles and the fracture morphology, the images were magnified (×20,000 and ×1000, respectively).

Differential scanning calorimetry (DSC) measurements were performed using a Netzsch DSC 204 to investigate nonisothermal crystallization kinetics in the cooling mode from the molten state. All tests were performed in nitrogen atmosphere. For each test, the sample was heated from 20 to 200 °C at a rate of 10 °C/min and then maintained at 200 °C for a period of 10 min to destroy any residual nuclei and to ensure an identical thermal history. The specimen was subsequently cooled down to 20 °C at three different cooling rates, including 5, 10 and 20 °C/min. The exothermic crystallization peak and crystallizing curves were recorded.

Polarizing light microscope (PLM) (Leitz Laborlux 12 Pols) equipped with a video camera and an optical hot stage was used to observe the process of isothermal crystallization and crystal morphology. The samples were first annealed at 200 °C for a period of 3 min, and then quickly cooled to 130 °C at a cooling rate of 90 °C/min. The size of the growing spherulites was recorded at a certain interval with an image processor.

The rheological measurements of the PP and PPCNs were carried out in a RHEOGRAPH 2002 high pressure rheometer at a temperature of 200 °C. Entrance angle of the capillary die was 180° and the value of *L*/*D* was 30, respectively. Since, we were just to compare the relative apparent viscosity of PP and its nanocomposites, the Bagley and Rabinowitch corrections were not performed.

Thermogravimetric (TG) measurements were performed to inspect the thermal stability of PP and its nanocomposites. The samples both in air and nitrogen (N_2) atmosphere were heated from room temperature to 550 °C at a rate of 10 °C/min.

Mechanical properties were studied at room temperature on an Instron 4302 tension machine (Canton, MA, USA) with specimen dimensions of 25 mm×6.5 mm×1 mm. The notched Izod impact strength was obtained with an Izod machine. For these tests, at least five samples were measured.

3. Results and discussion

3.1. Evaluation of dispersibility of the clay in PPCNs

XRD patterns of OMMT and PPCNs are shown in Fig. 2. In terms of Bragg equation, i.e. $\lambda = 2d_{hkl}\sin 2\theta$, 2θ and d_{001} are listed in Table 2. It can be seen that the (001) plane peak of OMMT is about 3.75°, which is equivalent to a based spacing of 2.354 nm. While the (001) plane peak of OMMT in the PPCN-0 is 2.42°, shifting to lower angle in contrast to OMMT and corresponding to the interlayer space of about 3.647 nm. The increase of the interlayer space from 2.354 to 3.647 nm means that an intercalated nanocomposite is produced during direct extrusion processing. Such a phenomenon may be ascribed to the fact that PP-*g*-MA molecules intercalate into the interspaces of OMMT and make its layer distance enlarged, which thereby affords enough spaces for the long chains of PP to intercalate into crystal interlayer of OMMT. As can be seen

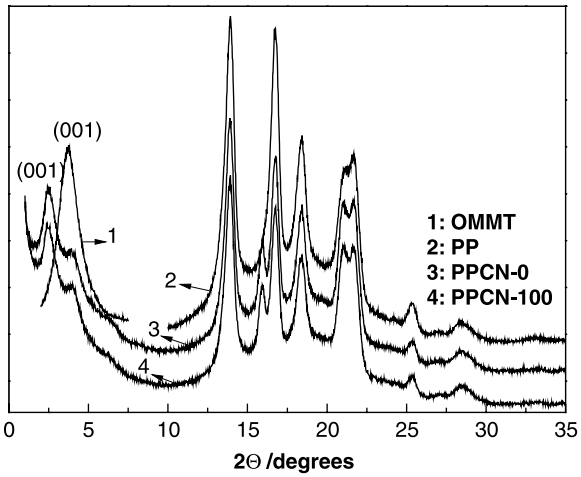

Fig. 2. XRD patterns of OMMT, PP and its nanocomposites.

Table 2
XRD parameters of OMMT, PP and its nanocomposites

Samples	2θ (°)	*d* (nm)	Crystal plane
Pure OMMT	3.75	2.35	001
OMMT in PPCN-0	2.42	3.65	001
PPCN-0	13.86	6.38	110
	15.94	5.56	300
	16.72	5.30	040
	18.38	4.82	130
	21.03	4.22	111
	21.73	4.09	131
OMMT in PPCN-100	2.38	3.71	001
PPCN-100	13.87	6.38	110
	16.02	5.53	300
	16.74	5.29	040
	18.38	4.82	130
	21.04	4.22	111
	21.73	4.09	131
Pure PP	13.92	6.36	110
	16.75	5.29	040
	18.40	4.82	130
	21.11	4.21	111
	21.62	3.68	131

from the Table 2, the pattern of PPCN-100 shows a basal peak $2\theta = 2.38°$ ($d_{(001)} = 3.704$ nm), while the 001 plane peak of PPCN-0 is 2.42° ($d_{(001)} = 3.674$ nm). So there is no evident difference in crystal interlayer of OMMT between PPCN-100 and PPCN-0, implying that the ultrasonic oscillations have a little effect on the extent of intercalation in nanocomposites.

From XRD results, we can still observe that there is a characteristic 2θ peak at 15.8° in PPCNs, corresponding to the structure of β phase of PP matrix. Whereas no sign of this peak can be detected in pure PP, except for the characteristic peaks of α phase at 14.0° (110), 17° (040), 18.6° (130) and about 21° (111,131). In addition, no difference in crystal phase between PPCN-0 and PPCN-100 can be seen. Therefore, loading a small amount of OMMT particles can make partial α phase transform into β phase, and ultrasonic oscillations have not any visible effect on the crystal phase.

From the TEM images, a better vision of intercalated structure in the nanocomposites can be gained. As it is shown in Fig. 3(c) and (d), the alternating dark and light regions, corresponding to OMMT and PP matrix, respectively, demonstrate intercalated structure of OMMT in PPCNs, which is consistent with the results of XRD analysis. Though the layer distance increases, the silicate layers still maintain ordered stacks in the PPCNs. In PPCN-0, the OMMT particles form bigger congeries and present the spatial-linked like structure as shown in Fig. 3(a) and (c). Several bundles of intercalated silicates assemble together because the edges of the silicate layers flocculate and appear self-assembled structure in PPCN-0. Whereas, the clay particles are finely dispersed in the polymer matrix of PPCN-100 and every bundle of intercalated silicates is thinner than that in PPCN-0 (as shown in Fig. 3(b) and (d)). Since, PP is an unpolar polymer, it is difficult to achieve an exfoliated nanocomposite. Consequently, just a little silicate layers are exfoliated in PPCN-100, which cannot be reflected in XRD. Therefore, the introduction of ultrasonic irradiations into PPCNs cannot greatly promote the extent of intercalation, but it can effectively prevent the silicate clay from assembling or flocculating.

3.2. Crystallization behavior and morphology

The crystallization exotherms of PPCN-100 as an example at various cooling rates (5, 10 or 20 °C/min) are presented in Fig. 4. From these curves, some useful data can be obtained to describe their nonisothermal crystallization behavior, such as the crystallization peak temperature (T_c) at which PP possesses the fastest crystallization rate, the beginning crystallization temperature (T_{onset}), the crystallization enthalpy (ΔH_c) which indirectly characterize crystallinity, the half-peak width (ΔW), and the degree of supercooling (ΔT) which is the result of melt point temperature subtracting T_c. Crystallization parameters of pure PP, PPCNs obtained from DSC curves are all listed in Table 3.

It is evident from Fig. 4 and Table 3 that the exothermic peak of each sample shifts to lower temperature and the crystallization temperature range becomes broader as the cooling rate increases. For an example of pure PP, the crystallization peak temperature is about 387.5 °C when the cooling rate is 5 °C/min, while at a cooling rate of 20 °C/min it is about 9 °C lower. A similar

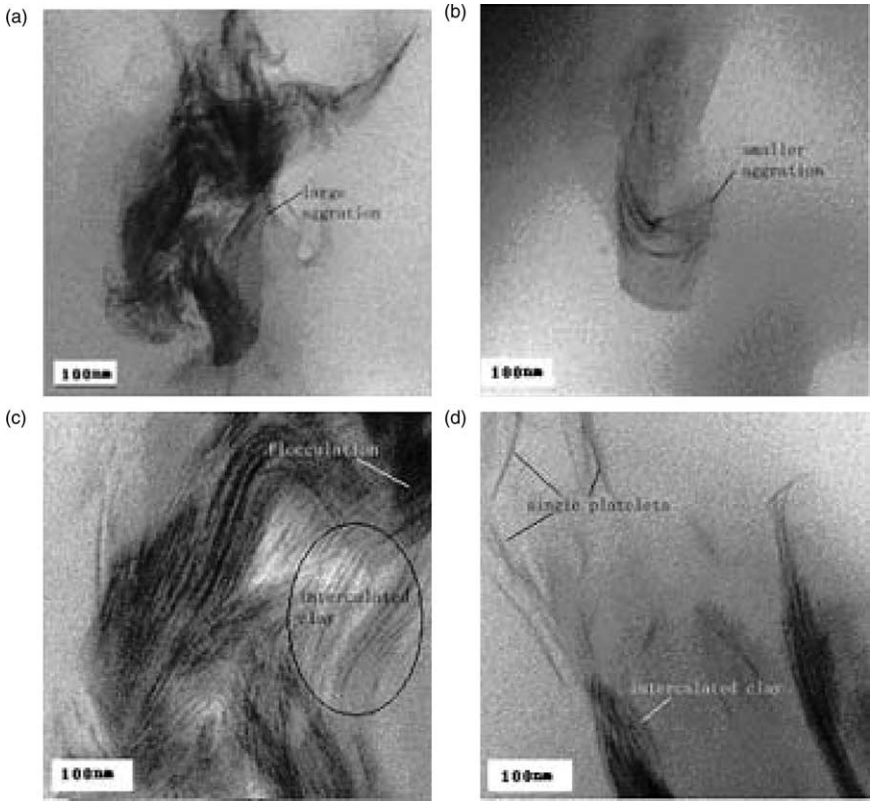

Fig. 3. Transmission electron micrograph images of the nanocomposites: (a) and (c) PPCN-0, (b) and (d) PPCN-100.

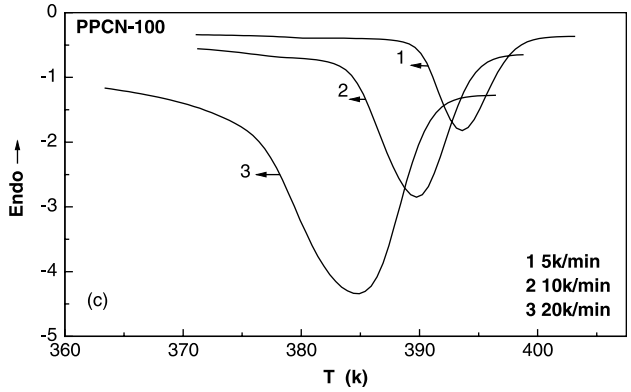

Fig. 4. DSC cooling curves for PPCN-100 nanocomposite at various cooling rates.

Table 3
Crystallization parameters of pure PP, PPCNs obtained from DSC curves

Sample	ϕ (K/min)	T_{onset} (K)	T_c (K)	ΔT (K)	ΔH_c (J/g)	ΔW (K)	$t_{1/2}$ (s)
PP	5	390.6	387.5	50.7	82.0	3.5	105
	10	388.4	384.5	54.0	81.8	5.2	70.8
	20	381.2	378.7	62.7	78.8	9.3	37.2
PPCN-0	5	397.9	393.4	45.3	96.4	5.1	113.4
	10	394.6	389.5	49.3	95.7	7.1	54
	20	390.8	384.2	55.5	90.3	11.1	34.2
PPCN-100	5	398.1	393.6	44.8	99.1	4.8	113.4
	10	394.7	389.7	48.7	98.3	6.3	60.6
	20	390.9	384.6	56.2	98.9	9.7	40.8

behavior is also observed in the nanocomposites as the cooling rate increasing. Compared with pure PP, T_{onset} and T_c of PPCNs shift to higher temperature, due to the fact that clay particles act as nucleation agents during the crystallization process of PP. At the presence of organic clay, ΔH_c of PPCNs also increases, indicating that the crystallinity of PP in the nanocomposite is higher than that in pure PP. The crystallization behaviors of PP filled with nanoparticles in the presence of ultrasonic oscillations are also studied and the results are compared with the nanocomposite prepared without ultrasonic oscillations. As shown in Fig. 4(b) and (c), after introducing ultrasonic oscillations into PPCNs, T_c and T_{onset} shift slightly to higher side, and the exothermic crystallization peaks are all sharper than that of PPCN-0. Then the width of crystallization peak (ΔW) of PPCN-100 is narrower than that of PPCN-0, which means ultrasonic oscillations can decrease the whole crystallizing time of PP chains.

Based on the assumption that the value of crystallinity is linearly proportional to the value of heat released during the crystallization, the crystallization exotherms as a function of temperature (dH_c/dT) can be obtained from dynamic crystallization experiment. According to the equation

$$X_t = \frac{\int_{T_{onset}}^{T} (dH_c/dT)dT}{\int_{T_{onset}}^{T_\infty} (dH_c/dT)dT}$$

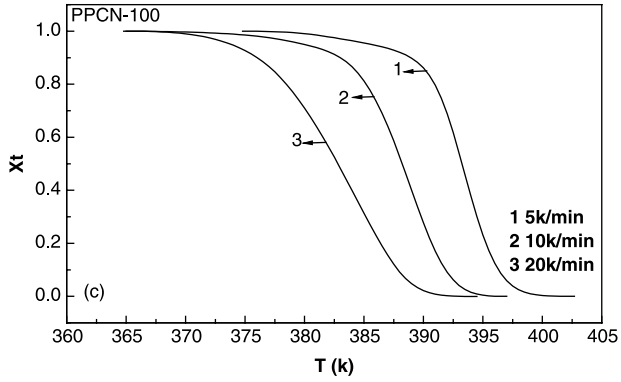

Fig. 5. Plots of X_t versus T for PPCN-100 nanocomposite at various cooling rates.

where T_{onset} and T_∞ denote the onset and the end of crystallization temperature, respectively, and T is the temperature at a certain crystallization time (t). We can obtain the development of the relative degree of crystallinity (X_t) as a function of crystallization temperature of PPCN-100 as an example at various cooling rates, as shown in Fig. 5. Using the following equation

$$t = \frac{(T_0 - T)}{\phi}$$

where ϕ is the cooling rate. Fig. 5 can be transformed into Fig. 6, which presents the relative degree of crystallinity (X_t) as a function of crystallization time of PPCN-100 as example, and the parameters obtained from Figs. 5 and 6 are listed in Table 3.

From Figs. 5 and 6, it can be seen that the curves of PP and PPCNs all fit for sigmoidal shape. Fig. 6 shows that the higher the cooling rate is, the shorter the time for completing crystallization is. The data listed in Table 3 show that the values of the half time of crystallization ($t_{1/2}$) for PPCNs are longer than that for PP at the cooling rate of 5 °C/min, whereas the trends reverse when the cooling rates are 10 and 20 °C/min. As we know the growth rate of crystallization is dependent on the competition between the rate of nucleation and the growth rate of crystal. Around the crystallizing temperature, lower temperature benefits nucleation, nevertheless crystal grows more quickly at higher temperature. When cooling rate is 5 °C/min, it is equivalent to crystallizing at

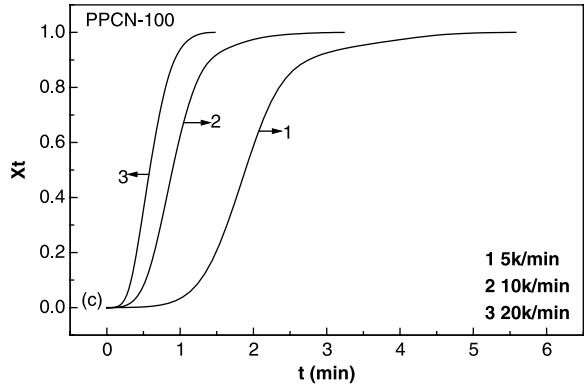

Fig. 6. Plots of X_t versus t for PPCN-100 nanocomposite at various cooling rates.

higher temperature, which makes against the nucleation but favors the crystal growth. Under this circumstance, clay acts as spacial barrier and blocks the motion and rearrangement of polymer chains. As a result, pure PP chains can move smoothly and crystallize fast, which causes that $t_{1/2}$ of pure PP is shorter than that of PPCNs. On the contrary, when the cooling rate is 10 or 20 °C/min, it is like to crystallize at lower temperature. Since, the clay acts as heterogeneous nucleating agent that is in favor of crystallization, as for PPCNs, the nucleation rate is fast while the crystal growth rate is slow. The competition of the two sides results in that the value of $t_{1/2}$ of PPCNs is smaller than that of PP. But for PPCN-100 and PPCN-0, they have similar nucleation mechanism. As can be seen in TEM images, the clay particles are finely and homogeneously dispersed in PPCN-100, which results in more spacial hamper and stronger interfacial interaction between PP chains and OMMT particles. Consequently, the crystallizing time of PPCN-100 is longer than that of PPCN-0. Thus, owing to the crystallizing complexity, the different

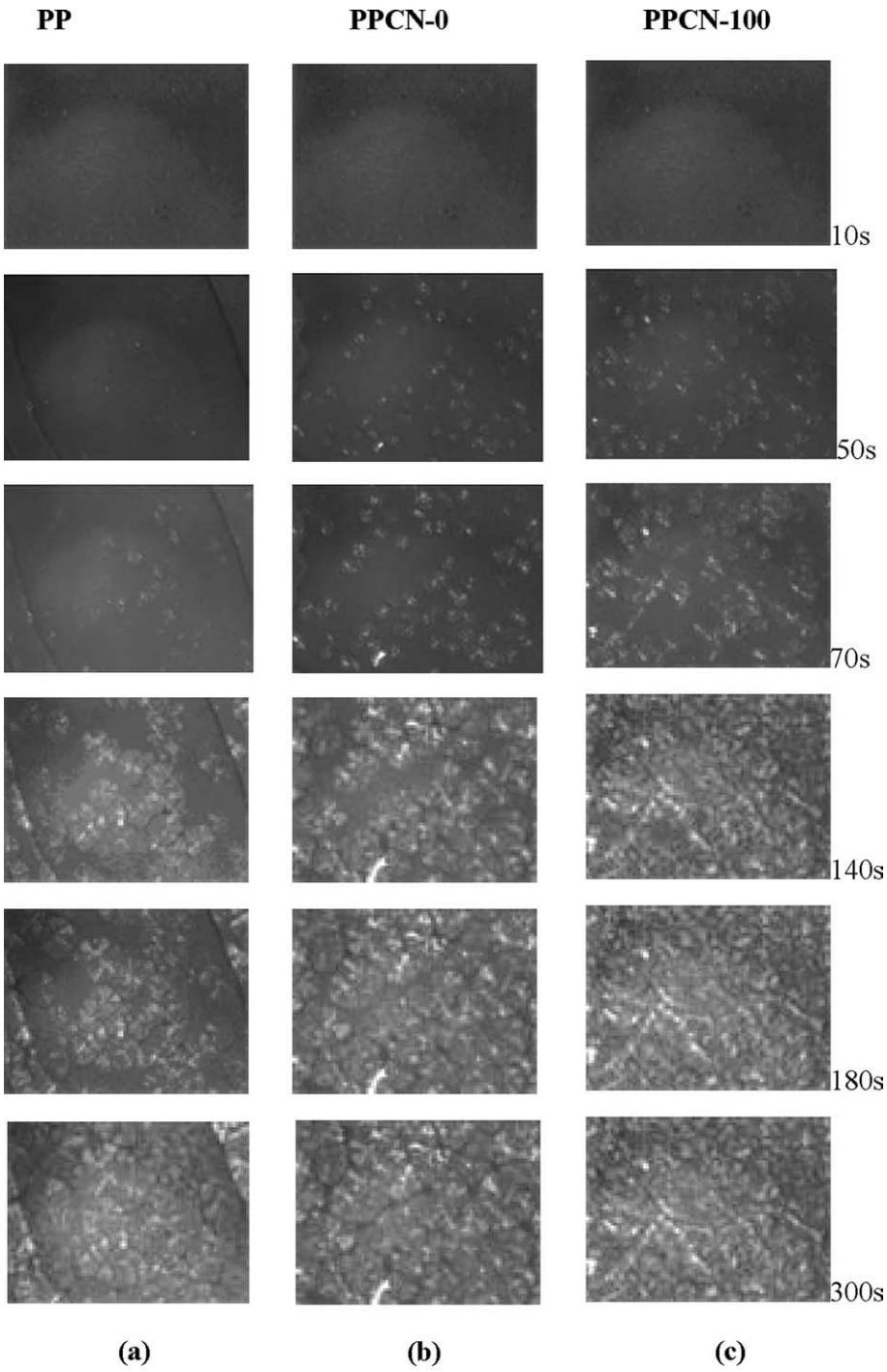

Fig. 7. (A) Polarized optical microscope showing the morphology of crystal of PP and PPCNS at various time (photos (×500), crystallizing temperature 130 °C); (B) plots of diameter of spherulites versus crystallization time for PP and its nanocomposites during isothermal crystallization process at 130 °C.

dispersion of layered silicates and distinct interface interaction, it is complex for polymer chains to crystallize in PPCNs.

Fig. 7 shows the PLM photographs of PPCNs as well as that of pure PP during isothermal crystallization process at 130 °C. It is clear in Fig. 7 that the nucleation rate in PPCNs gets improved compared with that in PP, because of heterogeneous nucleation of OMMT particles. Induction period of PP, PPCN-0 and PPCN-100 is 40–50, 10–20 and <10 s, respectively. Because ultrasonic oscillations can produce local shear at melts so as to promote the nucleation intensity in PPCN-100 by contrast with PPCN-0 at the same content, the induction period of PPCN-100 is shorter. Nowacki [35] also observed this phenomenon. He reported that shear could greatly enhance the nucleation of crystallization, due to very high nucleation sensitivity and nucleation intensity increasing of crystallization in nanocomposites under shear. Since, crystal growth is ultimately limited by the meeting of spherulite boundary, which leads to an irregular final structure and smaller crystalline dimension. We almost cannot see any perfect spherulite shape in Fig. 7(c), but the intersections of Fig. 7(a) and (b) are still evident and clear, indicating the existence of perfect spherulite. And the average spherulite size of PP, PPCN-0 and PPCN-100 is about 46, 26 and 21 μm, respectively. Therefore, compared with others, PPCN-100 has the least crystallization time and final crystal size at 130 °C. It is well known that crystalline morphology significantly affects the mechanical properties. Because smaller crystal is prone to develop into crack to absorb impact energy, on the contrary, big spherulite is apt to form local stress, which makes material become brittleness. So the crystalline morphology of PPCN-100 is favorable for its mechanical properties.

3.3. Analysis of the viscosities of the nanocomposites

As can be seen in Fig. 8, the viscosities of PP and PPCNs decrease with increasing shear rate, indicating a feature of pseudoplastic flow. In nanocomposites, the viscosity strongly depends on the surface characteristics of nanoparticles. For PPCNs, OMMT particle possesses the property of lubrication due to its sandwich structure and immiscibility with PP matrix. So the interfacial adhesion between OMMT particles and PP matrix is weak. When a shear stress is exerted on the nanocomposite, there is interlayer slip between OMMT particles and PP matrix, which results in ineffective shear transfer [36]. Thus, after adding OMMT particles, the viscosity of PPCNs drops at the same shear rate compared with pure PP. For PPCN-100, the fine and even dispersion of OMMT particles can further boost lubricative effect of layered silicates, and its shear viscosity is further reduced compared with that of PPCN-0. Therefore, adding OMMT particles and applying ultrasonic oscillations can improve the processing performance.

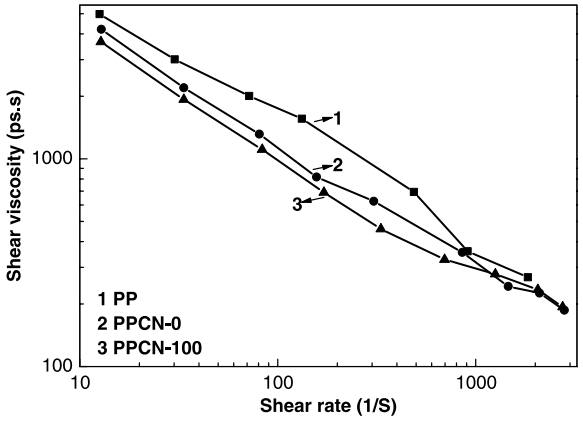

Fig. 8. Effect of shear rate on the viscosities of PP and PPCNs.

3.4. Thermal stability

In order to obtain indication on the heat barrier property and the oxygen role, the thermal stability of pure PP and its nanocomposites is studied both in nitrogen and air atmosphere by thermogravimetric analysis (TGA) in the present study. The results are shown in Fig. 9. The mass lost temperatures of 5% ($T_{-5\%}$), 10% ($T_{-10\%}$), 40% ($T_{-40\%}$), 50% ($T_{-50\%}$) and the extrapolation initial temperature (T_e) of degradation are listed in Table 4.

As shown in Fig. 9(A), the decomposition temperature of PPCNs shows an increment in contrast to virgin PP in nitrogen atmosphere. Because of layered structure of OMMT and the

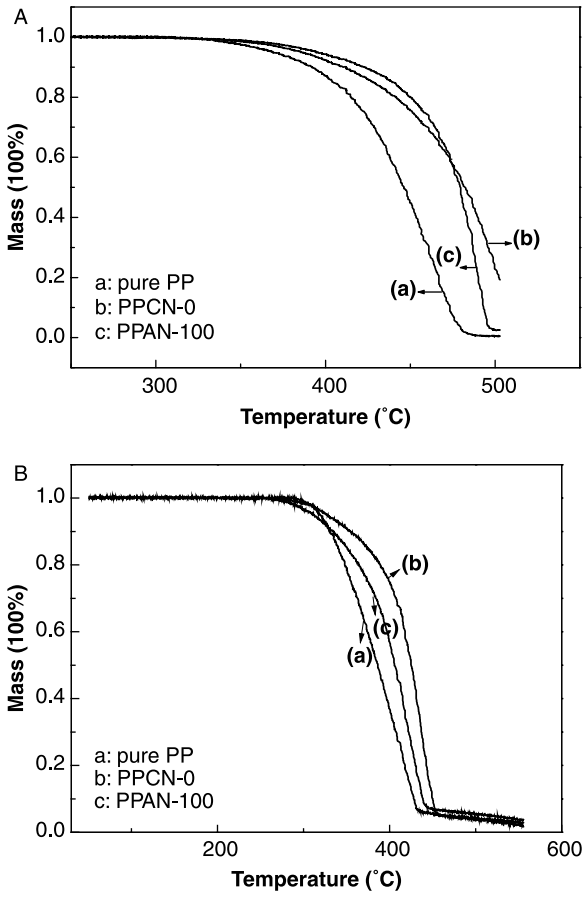

Fig. 9. The TG curves for PP and PPCNS: (a) PP, (b) PPCN-0 (untreated ultrasonically), (c) PPCN-100 (treated by 100 W ultrasound) ((A) at N_2 atmosphere, (B) at air atmosphere, respectively).

Table 4
Thermal stability of pure PP and its nanocomposites

Samples	$T_{-5\%}$ (°C)	$T_{-10\%}$ (°C)	$T_{-40\%}$ (°C)	$T_{-50\%}$ (°C)	T_e (°C)
In N_2					
PP	370.1	391.1	437.6	446.0	412.6
PPCN-0	386.4	409.2	472.9	482.1	443.6
PPCN-100	395.6	421.9	473.8	479.4	462.0
In air					
PP	320.7	332.8	373.9	384.5	336.5
PPCN-0	326.1	354.9	417.2	426.3	396.8
PPCN-100	309.3	333.6	395.9	408.0	370.4

restricted thermal motion of matrix molecules in the clay gallery, the clay acts as a heat barrier and enhances the overall thermal stability of the system. Additionally, there is an interesting phenomenon in the TGA curves of PPCN-0 and PPCN-100 in nitrogen atmosphere. Compared with PPCN-0, $T_{-5\%}$ and $T_{-10\%}$ of PPCN-100 are higher; however, the two curves show an intersection point at 477 °C, thereafter the decomposition temperature of PPCN-100 becomes lower than that of PPCN-0. Such a phenomenon can be interpreted in terms of even dispersion of OMMT in PPCN-100, which means that the matrix has more area to intimately contact with the clay crystalline layers. In the early stage of thermal decomposition, more heat is held in PPCN-100 system than that in PPCN-0. At higher temperature, in adding to 16-C alkyl quaternary ammonium bound to OMMT to degrade into free radical chains, which then may result in the initiated degradation of the chains of PP, the accumulated heat in the stacked layers of PPCN-100 can behave as a heat source to speed up the decomposition process, and the heat barrier of OMMT has a reversed effect on the thermal stability [37,38].

In air atmosphere, after adding OMMT particles, PPCN-0 exhibits a significant delay in weight loss by contrast with pure PP and PPCN-100 (as shown in Fig. 9(B)). However, PPCN-100 shows the lower thermal stability at the early stage of decomposition in air atmosphere. Because the decomposition takes place on the sample surface at the early stage, meanwhile in air atmosphere the sample surface contacts directly with oxygen, we postulate that the initial decomposition temperature significantly depends on the oxygen sensitive of the surface molecules. For PPCN-100, partial PP molecules degrade and become short chains under ultrasonic oscillations [39], which are more sensitive to oxygen and easier to be thermooxidated decomposition [38,40,41]. So PPCN-100 has early decomposition temperature. But at higher temperature, the clay still acts as a heat barrier and enhances the overall thermal stability of the PPCN-100. This interesting phenomenon will be further investigated in our latter work, especially the decomposition mechanism.

3.5. Mechanical properties and microstructure

The mechanical properties of pure polymers and nanocomposites are shown in Table 5. Commonly, the addition of clay in polymer will cause a decrease of elongation at break, even using small loading, but the ultrasonic oscillations can amend this disadvantage in our experiment. Compared with PPCN-0, there are sharp increases of 1300% in elongation at break, 19.8% in tensile strength, 24.3% in tensile modulus and 150% in impact strength in PPCN-100. However, compared with pure PP, elongation at break and impact strength of PPCN-100 both decrease, mainly because interaction between matrix and OMMT is relatively weak. We also calculate the standard deviation (SD) for each mechanical property (listed in Table 5). To explain the variation of mechanical properties and understand the mechanism, the microscope morphology and fracture morphology of PP and its nanocomposites are investigated by SEM analysis (as shown in Fig. 10).

The microscope morphology of PPCNs is shown in Fig. 10(a) and (b). It is clear that OMMT particles aggregate with a size about 200–300 nm, whereas, PPCN-100 shows the stacked clay particles with smaller average size less than 100 nm and the distribution of its particle size is much more uniform. This indicates that the ultrasound can obviously prevent the agglomeration and improve the dispersion of clay in polymer matrix. The fracture morphology of PPCN-100 greatly differs from that of PPCN-0 (as shown in Fig. 10(c) and (d)). There are many holes whose average size is about 2 μm in PPCN-0, showing a characteristic brittle fracture. However, polymer matrix of PPCN-100 forms micro-orientation structure corresponding to the

Table 5
Mechanical properties of PPCNS

Samples	Ultrasonic intensity (W)	Tensile strength (MPa), mean (SD)	Elongation at break (%), mean (SD)	Tensile modulus (MPa), mean (SD)	Impact strength (kJ/m^2), mean (SD)
PPCN-0	0	21.2 (0.51)	12.5 (4.52)	1299 (62.62)	14.1 (1.82)
PPCN-100	100	25.5 (0.24)	260.7 (17.76)	1614 (79.57)	35.1 (4.15)
PP	0	22.2 (0.23)	658.7 (45.31)	973 (64.15)	60.7 (7.44)

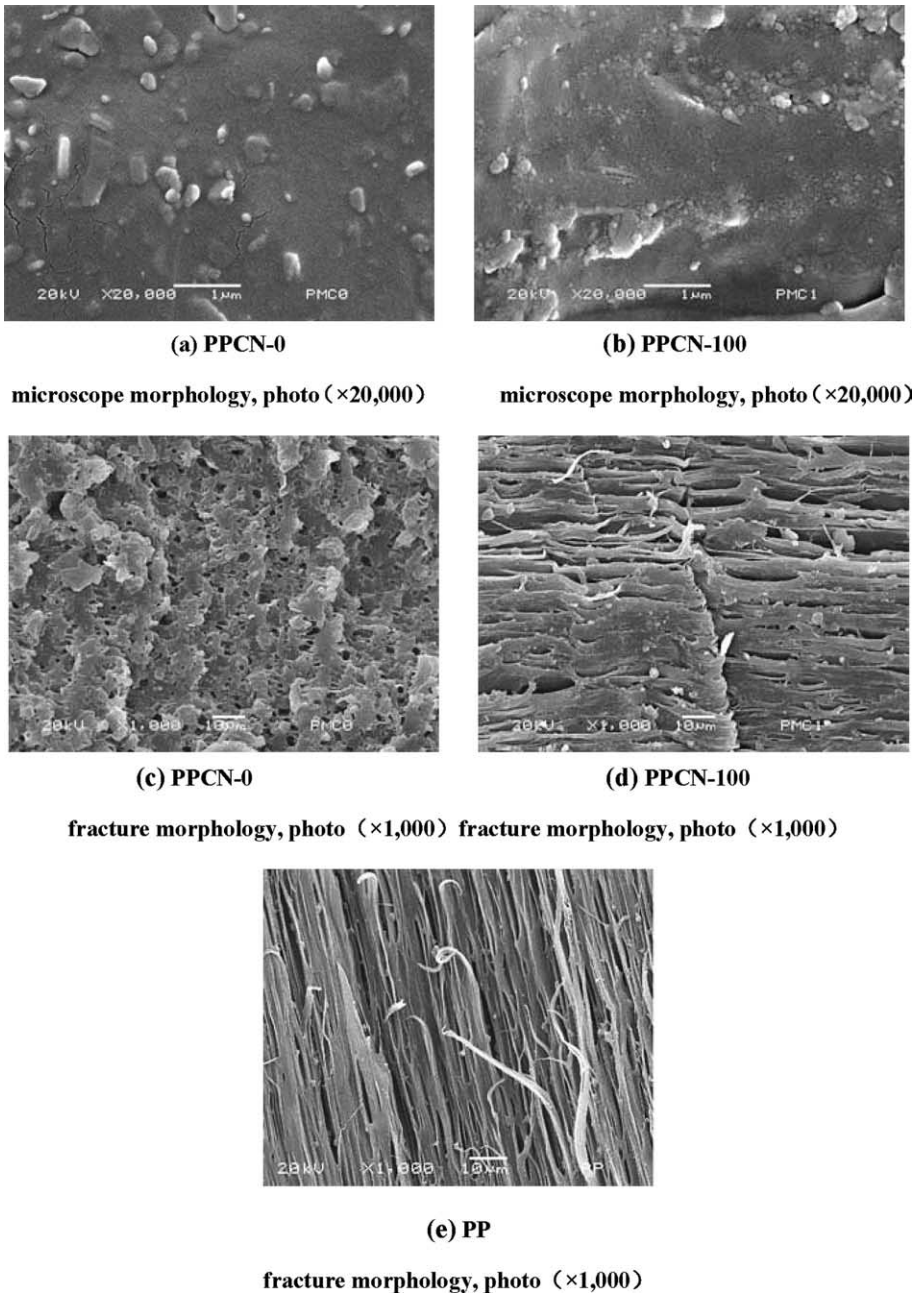

Fig. 10. SEM images of PP and PPCNS.

ductile fracture, which is also observed in pure PP (as shown in Fig. 10(e)).

As observed by TEM and SEM analysis, OMMT particle aggregations become smaller under ultrasonic irradiation, which ultimately leads to the increase of the interface action due to better overall dispersion of nanoparticles. The increase of the interface action is in favor of further adsorption and physical bond between the matrix and clay, therefore, the interaction is reinforced. When a stress is exerted on the polymeric nanocomposites, the OMMT particles will separate from the matrix, resulting in interfacial voiding as seen in SEM. Such a phenomenon benefits to the stress transformation between the two interfaces, so PPCN-100 can endure larger loading for longer time. On the contrary, because inorganic rigid particles do not possess plasticity, bigger aggregations of OMMT particles make the matrix phase thinner, leading to the easier fracture of matrix phase.

4. Conclusions

In summary, we have successfully prepared the PP nanocomposites with intercalated structure of the OMMT by melt intercalation via ultrasonic oscillations. Ultrasonic oscillations not only improve the dispersion effect of OMMT particles in PP matrix, but also diminish spherulite size of PP in nanocomposites. Therefore, ultrasonic oscillations in extrusion greatly improve the mechanical properties of the

nanocomposites, especially for the elongation at break and the impact strength. The elongation at break and impact strength of ultrasonicated nanocomposite are ca. 23 and 2.5 times as high as those of conventional nanocomposite. The shear viscosity of conventional nanocomposites is lower than that of the nanocomposites treated with ultrasound at low shear rate, and thermal stability of PP and its nanocomposites have different results whatever in N_2 and in air atmosphere. Adding OMMT particles can improve the thermal stability in N_2 and in air atmosphere. Compared with conventional nanocomposites, introducing ultrasound into the PP nanocomposites can make the decomposition temperature higher, but the thermal stability of ultrasonicated nanocomposite decreases in air.

Acknowledgements

The authors are grateful to the Special Funds for Major State Basic Research Projects of China (2005CB6238), National Natural Science Foundation of China (50233010, 20374037) for financial support of this work.

References

[1] Kurokawa Y, Yasuda H, Kashiwagi M, Oyo A. J Mater Sci Lett 1997; 16(20):1670–2.
[2] Delozier DM, Orwoll RA, Cahoon JF, Johnston NJ, Smith JG, Connell JW. Int SAMPE Tech Conf 2001;33:684–96.
[3] Tjong SC, Meng YZ, Xu Y. J Polym Sci, Part B: Polym Phys 2002; 40(24):2860–70.
[4] Liao M, Zh J, Xu H, Li Y, Shan W. J Appl Polym Sci 2004;92(5):3430–4.
[5] Vlasveld DPN, Vaidya SG, Bersee HEN, Picken SJ. Polymer 2005; 46(10):3452–61.
[6] Koo CM, Kim JH, Wang KH, Chung IJ. J Polym Sci, Part B: Polym Phys 2005;43(2):158–67.
[7] Tang Y, Hu Y, Wang S, Gui Z, Chen Z, Fan W. Polym Adv Technol 2003; 14(10):733–7.
[8] Yei D-R, Kuo S-W, Su Y-C, Chang F-C. Polymer 2004;45(8):2633–40.
[9] Agag T, Koga T, Takeichi T. Polymer 2001;42(8):3399–408.
[10] Xu Y, Brittain WJ, Xue C, Ronald K. Polymer 2004;45:3735–46.
[11] Maity AK, Nath D, Chakravorty D. Condens Matter 1996;8(31):5717–23.
[12] Chen W, Xu G, Yuan RZ. J Mater Sci Lett 1999;14(91):711–3.
[13] Liang ZM, Yin J, Xu HJ. Polymer 2003;44(5):1391–9.
[14] Vlasveld DPN, de Jong M, Bersee HEN, Gotsisa AD, Picken SJ. Polymer 2005;46(23):10279–89.
[15] Chaiko DJ. Chem Mater 2003;15(5):1105–10.
[16] Yua Y-H. Polymer 2003;44(12):3553–60.
[17] Limin L, Zongneng Q. J Appl Polym Sci 1999;71(7):1133–8.
[18] Kim K-N, Kim H, Lee J-W. Polym Eng Sci 2001;41(11):1963–9.
[19] Chung MJ, Jang LW, Shim JH, Yoon J-S. J Appl Polym Sci 2005;95(2): 307–11.
[20] Liu X, Wu Q. Polymer 2001;42(25):10013–9.
[21] Nam PH, Maiti P, Okamoto M, Kotaka T. Polymer 2001;42(23): 9633–40.
[22] Hasegawa N, Kawasumi M, Kato M, Usuki A. Macromolecules 1997;30: 6333–8.
[23] Usuki A, Kato M, Okada A. J Appl Polym Sci 1997;63:137–8.
[24] Kim JH, Koo CM, Choi YS, Wang KH. Polymer 2004;45(22):7719–27.
[25] Dennis HR, Hunter DL, Chang D, Kim S, Paul DR. Polymer 2001;42(23): 9513–22.
[26] Kim GM, Lee DH, Haffmann B, Kressler J, Stoppelmann G. Polymer 2001;42(3):1095–100.
[27] Chen G, Guo S, Li H. J Appl Polym Sci 2002;84:2451–60.
[28] Feng W, Isayev AI. Polymer 2004;45(4):1207–16.
[29] Kim H, Lee JW. Polymer 2002;43(8):2585–9.
[30] Jianling Z, Zhimin L, Buxing H, Tao J, Weize W, Jing C, et al. J Phys Chem B 2004;108(7):2200–4.
[31] Gul RJ, Wan PS, Hyungsu K, Wook LJ. Mater Sci Eng C 2004;24(1–2): 285–8.
[32] Artzi N, Nir Y, Narkis M, Siegmann A. J Polym Sci: Polym Phys 2002; 40(16):1741–53.
[33] Lee EC, Mielewski DF, Baird RJ. Polym Eng Sci 2004;44:1773–82.
[34] Li J, Zhao L, Guo S. Polym Bull 2005;55:217–23.
[35] Nowackia R, Monasseb B, Piorkowskaa E, Galeskia A, Haudinb JM. Polymer 2004;45(14):4877–92.
[36] Zhang B, Ding Y, Chen P, Liu C, Zhang J, Hea J, et al. Polymer 2005; 46(14):5385–95.
[37] Ray SS, Okamoto M. Prog Polym Sci 2003;28:1539–641.
[38] Billingham NC, Then ETH. A Kron. Polym Degrad Stab 1997;55:339–46.
[39] Hyungsu K, Wook LJ. Polymer 2002;8(43):2585–9.
[40] Iedemaa PD, Willems C, van Vliet G, Bunge W, Mutsers SMP, Hoefsloot HCJ. Chem Eng Sci 2001;56:3659–69.
[41] Chan JH, Balke ST. Polym Degrad Stab 1997;57:113–25.